Materials and Design 198 (2021) 109284

Contents lists available at ScienceDirect

Materials and Design

journal homepage: www.elsevier.com/locate/matdes

Preparation of sustainable fibers from isosorbide: Merits over bisphenol-A based polysulfone

Ho-Sung Yang [a], Seungwan Cho [a], Minkyung Lee [a], Youngho Eom [a,b], Han Gi Chae [c], Seul-A Park [a], Min Jang [a], Dongyeop X. Oh [a,d,*], Sung Yeon Hwang [a,d,*], Jeyoung Park [a,d,*]

[a] Research Center for Bio-based Chemistry, Korea Research Institute of Chemical Technology (KRICT), Ulsan 44429, Republic of Korea
[b] Department of Polymer Engineering, Pukyong National University, Busan 48513, Republic of Korea
[c] School of Materials Science and Engineering, Ulsan National Institute of Science and Technology (UNIST), Ulsan 44919, Republic of Korea
[d] Advanced Materials and Chemical Engineering, University of Science and Technology (UST), Daejeon 34113, Republic of Korea

HIGHLIGHTS

- Sustainable fiber from bio-based isosorbide is fabricated using a dry-jet wet spinning.
- Better water tolerance of bio-based polysulfone enables a compact fiber structure.
- The Bio-based fiber has a mechanical strength 2.3 times that of the petroleum-based fiber does.
- The potential use of a bio-based fiber in a wig application is demonstrated by its similarity to human hair.
- The thermal stability of the fiber is high enough to prevent damage at 200 °C.

GRAPHICAL ABSTRACT

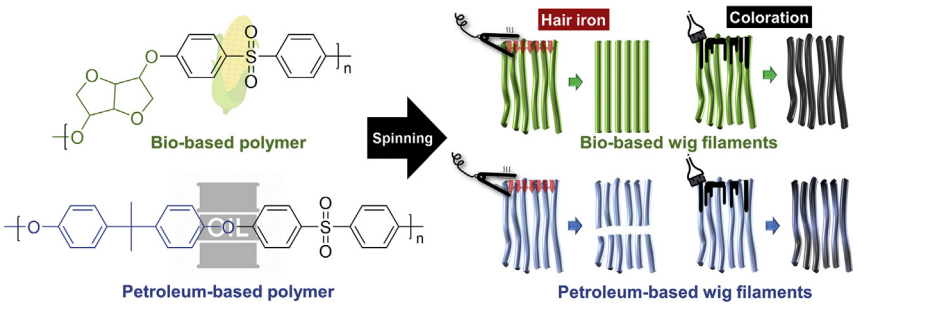

ARTICLE INFO

Article history:
Received 7 September 2020
Received in revised form 29 October 2020
Accepted 30 October 2020
Available online 4 November 2020

Keywords:
Isosorbide
Polysulfone
Bio-based fiber
Amorphous fiber
Wig filament
High thermal stability

ABSTRACT

To address environmental concerns related to the large volume of plastics currently used, high-performance, sustainable, and satisfactorily performing bioplastics can be a solution. Isosorbide (ISB)-based amorphous poly (arylene ether sulfone)s (PAESs) derived from biomass feedstocks instead of harmful aromatic petrochemicals, such as bisphenol-A (BPA), are promising novel materials. To expand the range of eco-friendly products, ISB-PAES microfibers (ISU) along with BPA-PAES-based microfibers (PSU) have been fabricated through dry-jet wet spinning. ISU is mechanically 2.3 times stronger (247 MPa) than PSU (106 MPa), which may be ascribed to the compact and homogeneous structure of ISU compared to the porous structure of PSU. This structural superiority is due to the polar ISB moiety, which improves the phase stability of the ISU spinning dope in water (a role of the coagulant). For potential wig applications, the diameter, strength, and moduli of ISU are well matched to those of human hair. In addition, ISU is easily colored and endures high temperatures better than current wig filaments. It survives at high temperatures without breaking down during hair iron treatment (200 °C).

1. Introduction

There is an increasing demand for the replacement of petrochemical processes and plastics with sustainable materials that alleviate serious environmental issues [1,2]. Petroleum-based raw materials, such as

* Corresponding authors.
E-mail addresses: dongyeop@krict.re.kr (D.X. Oh), crew75@krict.re.kr (S.Y. Hwang), jypark@krict.re.kr (J. Park).

https://doi.org/10.1016/j.matdes.2020.109284

bisphenol-A (BPA), biphenols, and styrenes, which are key monomers for the synthesis of engineering plastics and super engineering plastics (SEPs), may be harmful to human health [3–6]. Specifically, BPA acts as an endocrine-disrupting compound and can cause developmental and reproductive problems in humans [7–9]. Consequently, there is a reluctance to use products made of polycarbonate, polysulfone (PSU), and epoxy resin, which contain BPA, in consumer goods.

Sustainability is being increasingly highlighted in the polymer field. Sustainability refers to the ability of ecosystems and human civilization to coexist harmoniously, and green chemistry focuses on minimizing the generation of hazardous substances causing environmental pollution during the chemistry processes. Therefore, these concepts should be emphasized continuously to reduce environmental pollution that threatens the survival of mankind. Various efforts have been made to replace petroleum-based polymers with biopolymers [10–15].

It is noteworthy that biopolymers are defined as having all or some of their monomers derived from nature or biomass. Some biopolymers are not biodegradable. Otherwise, biodegradable polymers are also called biopolymers, regardless of their source. For example, although poly(butylene succinate) [16] can be synthesized from petroleum-based monomers, it is considered a biopolymer owing to its biodegradability. In summary, all biodegradable polymers can be called biopolymers, regardless of their sources, but not all biopolymers are biodegradable.

Sustainable poly(arylene ether sulfone) (PAES) as an amorphous SEP has been developed using an isosorbide (ISB) monomer derived from biomass feedstocks [17,18]. It is noteworthy that ISB-PAES is a non-biodegradable biopolymer. ISB has been demonstrated to be safe and has been used in pharmaceutical and cosmetic applications [19,20]. It has also been used in additives, particularly for flame retardants [21], and dimethyl isosorbide, one of the simplest derivatives of isosorbide, is used as a bio-based green solvent [22]. ISB-PAES exhibits excellent mechanical performance (tensile strength of 78 MPa), high thermal phase change (glass transition temperature (T_g) of 212 °C), low coefficient of thermal expansion (CTE; 23.8 ppm K^{-1} at 30–80 °C), and good biocompatibility.

Amorphous SEPs composed of high T_g polymers can be used at temperatures above 150 °C; hence, these plastic products have been used in energy-related devices [23–25], machine parts [26], composite materials [27–29], and membranes [30,31] owing to their excellent mechanical properties, thermal stability, electrical insulating properties, chemical and oxidative resistance, and low CTEs. However, few studies on the fabrication of solid fibers from amorphous SEPs have been reported [32].

A wig composed of artificial hair is a promising application of solid amorphous SEP fibers. Polyacrylonitrile (PAN), poly(vinyl chloride) (PVC), and poly(ethylene terephthalate) (PET) are generally used in artificial filaments. They undergo relatively low thermal phase change, with T_gs of 106, 76, and 80 °C for PAN, PVC, and PET fibers, respectively [33,34]. These materials cannot be used with hair irons as they operate at a high temperature (< 200 °C). Indeed, synthetic fibers for wig filaments have previously been reported to exhibit unsatisfactory thermal performance [35,36].

Moreover, PAN, PVC, and PET fibers are relatively difficult to dye at moderate temperatures because they lack chemical activity for typical dyes and possess compact structures [37–39]. Therefore, dye carriers [35,39], special treatment [40], co-monomers [41], or additives [42,43] containing dyeing sites are generally required for dyeing at temperatures around their T_gs. Furthermore, hazardous materials, such as gaseous hydrogen chloride and hydrogen cyanide, are emitted from PAN and PVC at around 120 °C [44] and 200 °C [45], respectively. In summary, characteristics such as amorphousness, high thermal stability, appropriate hydrophilicity, good mechanical properties, and a lack of skin toxicity are necessary for wig filament applications.

Micro-sized fibers have been fabricated using bio-based ISB-PAES and petroleum-based BPA-PAES, which are referred to as “ISU” and “PSU,” respectively, using a dry-jet wet spinning process, and the properties of these fibers were examined and compared. To determine whether ISU can be used in wig filaments, the thermomechanical properties and water-based coloration of these fibers have been examined. The diameters and strengths of ISU fibers were found to be similar to those of human hair [46–48]. In addition, the strength and thermal dimensional stability of ISU were superior to those of PSU; it did not break during hair iron testing (200 °C) and exhibited good coloration at 25 °C.

2. Experimental

2.1. Dope preparation

The preparation of materials and characterizations are described in the Supplementary Information. To remove moisture in ISB-PAES and BPA-PAES, each polymer powder was placed in a closed chamber at 100 °C for 9 h under nitrogen (purity: 99.999%) at a flow rate of 2 mL min^{-1}. After removing the nitrogen, the temperature was increased to 120 °C. Subsequently a 40 wt% solution was prepared by adding dimethyl sulfoxide (DMSO) without exposing the solution to air. The solution was stirred at 300 rpm for 3 h and degassed at 10 Torr and 100 °C for 1 h.

2.2. Fiber fabrication and heat drawing processes

Dope solutions were spun as microfibers (ISU and PSU) by dry-jet wet spinning under the experimental conditions described below. The dope was preheated to 70 °C and poured into a metal syringe heated to 70 °C. The solution was ejected through a nozzle using a gear pump. The spinning system was equipped with an eight-hole spinneret with 150-μm-diameter holes. The linear velocity of the polymer jet from the nozzle was set to 6 m min^{-1} and the air gap (the distance between the nozzle and the coagulation bath) was set to 1.5 cm. The coagulation bath was filled with deionized (DI) water and maintained at 10 °C. Fibers formed in the coagulation bath were passed through a guide roller at 9 m min^{-1} and were wound up on a bobbin installed in a winder at 9 m min^{-1}. The spinning draw ratio was 1.5. To remove residual DMSO within the fibers, the fiber-wound bobbins were stored in DI water for 5 d before being subjected to the heat drawing process. The bobbin was installed in an unwinder and the fibers passed through a guide roller, as well as three separate heat rollers, an additional guide roller, and a winder. The temperatures of the heat rollers were set to 100, 150, and 180 °C. The heat draw ratios were two and three, so the total draw ratios (TDRs, spinning draw ratio × heat draw ratio) were 3.0 and 4.5. Each TDR is indicated by a number next to the sample code (e.g., ISU-1.5, ISU-3.0, ISU-4.5, and PSU-1.5, PSU-3.0, PSU-4.5).

3. Results and discussion

3.1. Spinning, mechanical properties, and morphologies of amorphous fiber

The chemical structures of ISU and PSU, the spinning process, and their potential applications as wig filaments are schematically illustrated in Fig. 1. ISB-PAES and BPA-PAES dissolved in DMSO were spun into microfibers by dry-jet wet spinning. The prepared dope was poured into a syringe connected to a gear pump. The polymer jets ejected from the nozzle passed through an air gap and solidified in a coagulation bath, and the formed fibers were wound using a winder. To the best of our knowledge, this is the first time that bio-based amorphous SEP fibers have been fabricated. Moreover, the mechanical and thermal properties of ISU are sufficient for comparison with those of previously reported fibers fabricated from crystalline SEPs, such as poly(phenylene sulfide) [49] and poly(ether ketone) [50,51].

Representative stress–strain (S—S) curves and relationships between fiber diameter, strength, Young's modulus, and TDR are shown in Fig. 2. Properties of typical human hair are also shown for comparison with those of fabricated fibers [45]. As shown in the S—S curves

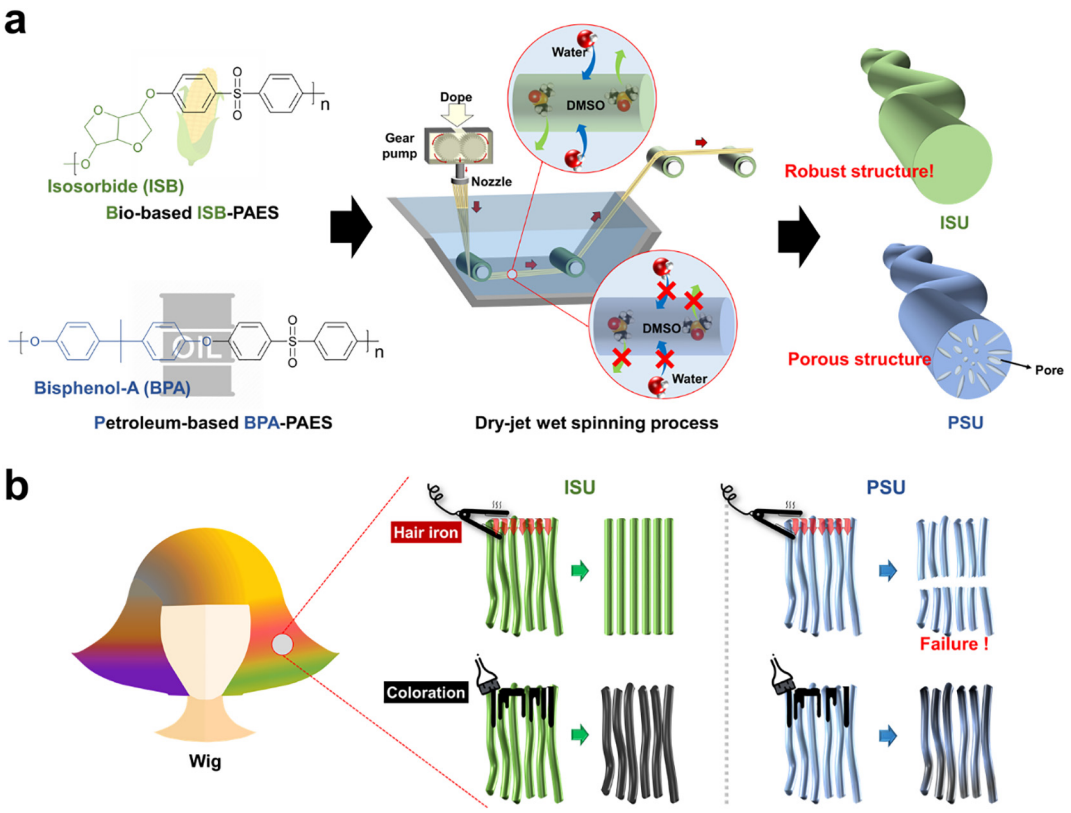

Fig. 1. (a) Process for the fabrication of bio−/petroleum-based amorphous fibers. (b) Representative heat stability and coloring characteristics for wig applications.

(Fig. 2a), the ISU fiber is more ductile, with a higher failure strain than the PSU fiber at a low TDR of 1.5, whereas it was stronger and stiffer at a high TDR of 4.5. The ductility-to-stiffness variations in the mechanical properties of the ISU fiber reveal that its performance is easily tailored by the post-fiber drawing processes. The PSU fiber diameter was much larger than that of ISU at each TDR (Fig. 2b and Table S1). The average diameters of the ISUs and PSUs were determined to be 72, 48, 40 μm, and 103, 57, 50 μm, at TDRs of 1.5, 3.0, and 4.5, respectively. A single strand of ISU-4.5 exhibited a strength of 247 MPa, which is 2.3 times higher than that of PSU-4.5 (106 MPa) (Fig. 2c). Young's modulus of the ISU was higher than that of the PSU (Fig. 2d) at each TDR. From the perspective of artificial hair applications, the diameter, tensile strength, and modulus of ISU-4.5 are well matched to those of human hair [47,52,53].

To elucidate the factors responsible for the excellent mechanical properties of ISU compared to PSU, their cross sections were examined by field-emission scanning electron microscopy (SEM), as shown in Fig. 3. All fibers had circular cross sections without distorted or deformed contours, which implies that coagulation proceeded simultaneously in all radial directions [54]. Nonetheless, there are large differences in the cross-sectional morphologies of the ISU and PSU fibers, in contrast to their surfaces. All fibers exhibit smooth surfaces devoid of pores and cracks (Fig. S2). The ISUs have compacted structures with little difference between their shells and cores, while the PSU fibers have clear boundaries between their compacted shells and porous cores. This is evident in the magnified SEM images (Fig. S3). The high porosities as well as the clear structural discrepancies between the shell and core components of the PSU fibers engender them with inferior mechanical properties. The evident PSU core-shell structure is the result of rapid solidification of the spinning dope during the coagulation process. The rapid evolution of the stiff shell structure of the PSU severely impedes the diffusion of the solvent (DMSO) and the coagulant (water) out and in the PSU. Consequently, residual solvent remains, leading to high porosity for PSU. This porous structure leads to inferior mechanical properties and larger fiber diameters compared to those of the ISUs. Meanwhile, the low porosities and relatively homogeneous structures of the ISUs demonstrate that they undergo gradual and stable fiber formation during coagulation.

3.2. Water tolerance of the dopes and the microstructures of the amorphous fibers

The extent to which the coagulant affects the dope solution is a major concern. As mentioned above, the cross-sectional fiber morphology is predominantly determined by the phase change behavior of the spinning dope during coagulation. The compacted structure of ISU reveals gradual solidification, whereas the core-shell structure of PSU is the result of rapid solidification. In this regard, it was postulated that ISB-PAES solutions are more tolerant to the coagulant (water) than BPA-PAES solutions; hence, their water tolerances were rheologically evaluated (Fig. S4). The storage/loss moduli (G'/ G“) for the 40 wt% ISB- and BPA-PAES dope solutions and 1 wt%-water added solutions were compared. These water-containing solutions are referred to as “ISB-PAES/W" and “BPA-PAES/W.” The plots of G' and G" versus angular frequency (ω) reveal that the ISB-PAES dopes are affected little by the addition of 1 wt% water, indicating negligible phase change. On Meanwhile, the BPA-PAES dopes exhibit distinct changes in rheology, with substantial increases in G' observed in the low-frequency range. In addition, the incorporation of water results in the reduction of the initial slopes of the G' curves, from 1.19 to 0.74, indicative of a deterioration in solution homogeneity (an ideal homogeneous solution exhibits an initial slope of 2 in its G' curve) [55].

To clearly visualize the water tolerance of the 15 wt% ISB-PAES and BPA-PAES solutions, a simple experiment that mimics the coagulation process (Fig. 4 and Movie S1) was performed. Precipitation occurred in both solutions as the first drop of water was added (10 μL, 0.14 wt%

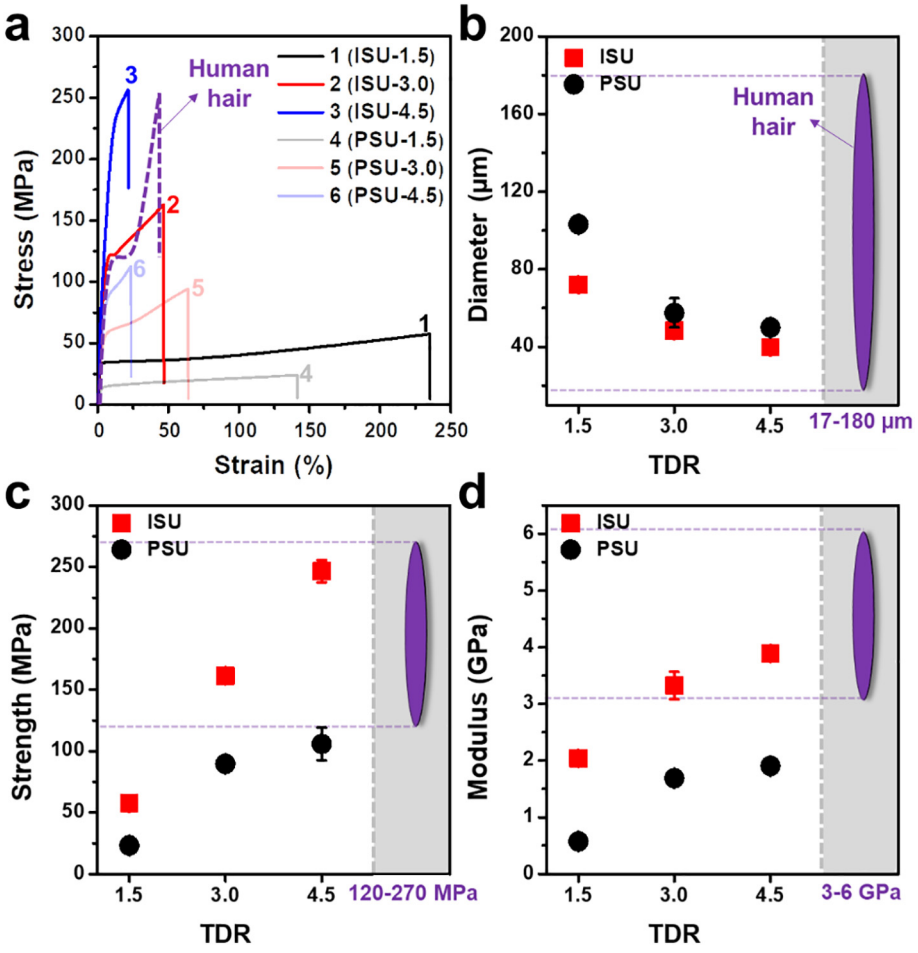

Fig. 2. Comparison of (a) stress-strain curves, (b) diameters, (c) strength, and (d) moduli of ISUs and PSUs as a function of total draw ratio. Data for human hair are indicated in purple.

per total solution), with the BPA-PAES solution exhibiting more precipitation than the ISB-PAES solution. The precipitate in the BPA-PAES solution formed a film-like shape on the surface when a second water drop was added to the solution (30 s interval), after which additional water drops were unable to penetrate into the BPA-PAES solution, resulting in continuous film thickening. After the last water drop (1.27 wt% per final solution) was added, the precipitate in the ISB-PAES was redissolved in 4 min, while the film on the surface of the BPA-PAES solution became thicker (Figs. 4b and c). Similarly, fast coagulation of the BPA-PAES shell in the dry-jet wet spinning process prevents additional coagulant from entering the PSU; consequently, the core becomes less coagulated and a porous structure develops in the PSU because of the presence of residual solvent.

The excellent water tolerance of ISB-PAES compared to BPA-PAES can be theoretically predicted using solubility parameters based on Hoftyzer–Van Krevelen group contribution theory [56,57]. The solubility parameters (δ) of ISB-PAES and BPA-PAES repeating units were calculated to be 24.96 and 23.75, respectively (Table S2), which are far below that of water (48); hence, both materials are insoluble in water. Further, δ and δ_H (δ for the hydrogen bonding contribution) of the ISB moiety (δ 25.15 and δ_h: 12.62) were higher than those of the BPA moiety (δ: 22.24 and δ_h: 4.38) (Table S3), which implies that the ISB moieties incorporated in the ISB-PAES chains can be more easily hydrated than the BPA moieties in the BPA-PAES chains. It is noteworthy that the bending angle of ISB is well matched to that of water [58]. In addition, the enhanced polarity of ISU, which results from the presence of two oxygen atoms in each alicyclic ring, improves the solubility of ISB-PAES in DMSO during dope preparation. Hence, the better chemical affinity of the partially polar ISB-PAES for the solvent and its contrasting coagulant behavior compared to that of the non-polar BPA-PAES resulted in higher spinnability and remarkable fiber properties.

The fibers were microstructurally analyzed by two-dimensional wide-angle X-ray scattering (2D-WAXS), as shown in Figs. 5 and S5. A bundle consisting of eight filaments was used in this experiment, with the fiber axes arranged in the horizontal direction. Sharp diffraction spots corresponding to a crystalline structure were not observed at a TDR of 1.5, with only halos appearing in the 2D-WAXS images of both fibers, consistent with amorphous structures. The halos narrowed and formed arcs with increasing TDR, indicative of increasing fiber axis orientation. Considering that the ISU arcs were flatter than the PSU arcs at TDRs of 3.0 and 4.5, the ISUs are better oriented along the fiber axis than the PSUs. Moreover, meridionally (lateral fiber section) extracted plots from the 2D-WAXS images show a significant reduction in intensity for ISU with increasing TDR compared to PSU (Figs. S5e and f). To quantify orientation, the Herman's orientation factors of the fibers (Fig. 5c) were calculated from azimuthal plots (Figs. S5g and h) extracted from the 2D-WAXS images at $2\theta = 11–16°$ and $\Phi = 0–90°$, where θ and Φ are the Bragg angle and azimuthal angle, respectively, using eqs. (S1) and (S2). The Herman's orientation factors of both fibers increased with increasing TDR (ISUs: 0.39 → 0.42 → 0.44; PSUs: 0.37 → 0.38 → 0.41), and the ISUs were more oriented than the corresponding PSUs at all TDR values. Generally, quick coagulation causes the formation of poorly oriented fibers due to residual solvent that acts as a defect that hinders orientation in the fiber axis direction [59–61].

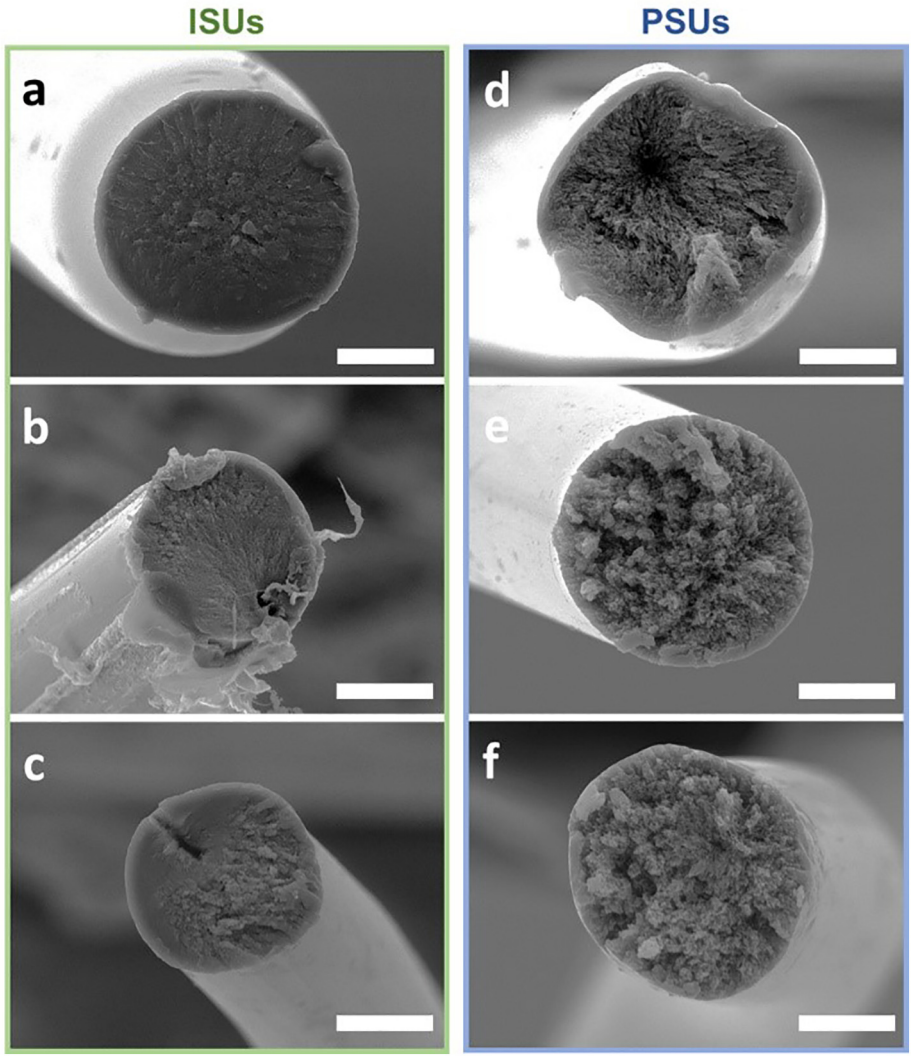

Fig. 3. Cross-sectional SEM images of fibers as a function of the total draw ratio (a: ISU-1.5, b: ISU-3.0, c: ISU-4.5, d: PSU-1.5, e: PSU-3.0, f: PSU-4.5; scale bar: 20 μm).

3.3. Trapped solvent and thermal stabilities of amorphous fibers

To determine the amounts of water and DMSO trapped inside the fibers, they were subjected to thermogravimetric analysis (TGA) and differential thermogravimetry (DTG) in the 25–300 °C range (Fig. S6). Clearly, the ISUs absorb more water during coagulation than the PSUs. The amount of water absorbed by each ISU, which was calculated by integrating the DTG peaks at 25–100 °C, was 2.27, 1.52, and 1.45% at TDRs of 1.5, 3.0, and 4.5, respectively. Less water is absorbed with increasing TDR because further drawing squeezes out the water within the ISU. The amount of water absorbed by the PSUs was determined to be almost 0%. The differences in the amounts of water absorbed by the two types of fiber are the result of their different chemical structures. Meanwhile, residual DMSO was determined from changes in the peaks in the 190–260 °C range (the boiling point of DMSO is 189 °C) in the TGA and DTG traces. Considering that the TGA and DTG traces of raw BPA-PAES showed no significant weight reduction at 190–260 °C (Fig. S7), it is reasonable to conclude that the peaks observed at 190–260 °C for the PSUs are related to DMSO; these peaks were more prominent for the PSUs than the ISUs, which indicates that the PSUs contain more residual DMSO. The amounts of DMSO in the ISUs were determined to be 0.28, 0.23, and 0.12% at TDRs of 1.5, 3.0, and 4.5, respectively, while the PSUs values were 0.65%, 0.58%, and 0.39%, respectively. The PSUs contain more DMSO than the ISUs because the DMSO in the PSU core cannot flow out of the fiber because of its quickly formed shell.

The temperatures at which the weights of ISU-4.5 and PSU-4.5 were decomposed by 5% ($T_{d5\%}$) were compared with those of PAN, PVC, and PET fibers used as wig filaments (Fig. S6g) [62]. The $T_{d5\%}$ of ISU-4.5 is 401 °C, which is higher than those of PAN, PVC, and PET fibers but lower than that of PSU-4.5 (497 °C). The higher bond dissociation energy of the BPA units increases the stability of the polymer during heating [63]. However, the thermal stability of ISU is sufficient to merits its use over conventional wig filaments because PAN and PVC emit hazardous gases at high temperatures [44,45]. Differential scanning calorimetry confirmed that ISU and PSU fibers are amorphous, as shown by the 2D-WAXS results (Fig. S8). The T_g values of all ISUs were similar, at ~235 °C, which are higher than those of the PSUs (~185 °C); no significant differences were observed for the different TDRs. The T_g values of the prepared fibers are higher than those of PAN [33], PVC [34], and PET [34] fibers (Fig. S9a). Thus, it is expected that the ISU fibers are thermally stable against potential damage when treated with a hair dryer or iron.

The CTE values of the fibers determined by thermomechanical analysis (TMA) at 30–80 °C indicate that ISU-4.5 has a higher thermal dimensional stability than an ISB-PAES film and PSU-4.5, owing to the fiber orientation and the stronger geometric constraints of the fused

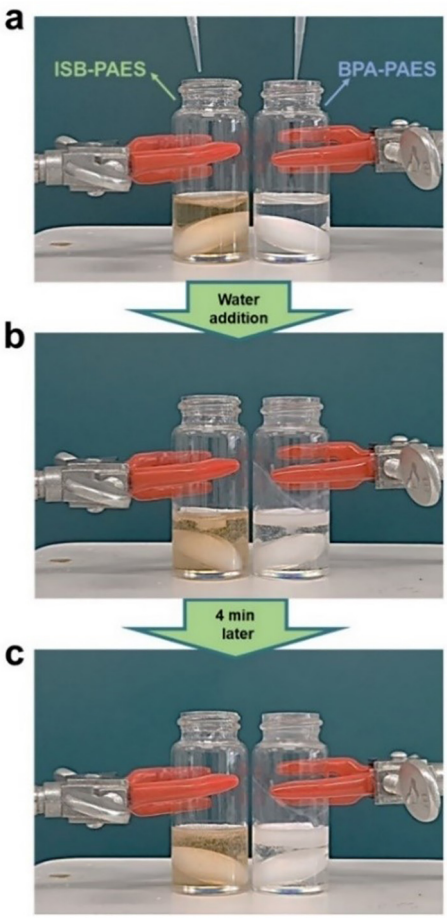

Fig. 4. Observing changes in the appearances of ISB-PAES and BPA-PAES solutions (15 wt %) upon the addition of water (1.27 wt% per total solution). (a) Initial states before water addition, (b) states after water addition, and (c) states 4 min after the final addition of water (see Movie S1).

aliphatic bicyclic ring in ISB than the planar benzene structure in BPA (Fig. S10) [17,18]. Consequently, ISU requires more energy for its polymer chains to move than PSU. This explanation is consistent with the observation that the ISUs exhibit higher initial moduli than the PSUs (Fig. 2d).

To visualize the difference in the thermal stabilities of ISU-4.5 and PSU-4.5, they were subjected to thermal stability experiments using a heat gun set to 200 °C (Fig. S9b and Movie S2). A 2.5-cm-long bundle of eight filaments was used in each experiment, with 10-g dangling weight along each fiber axis. While ISU-4.5 endured heat for 600 s without breaking, PSU-4.5 stretched by 14% immediately prior to breakage after 33 s. This experiment was conducted two more times with the same ISU-4.5 bundle. Notably, the used ISU-4.5 endured another 600 s under the same experimental conditions as well as a third 600 s with a 20-g dangling weight without breaking (Fig. S11 and Movie S3).

3.4. Application as artificial hair

Fig. 1b schematically depicts the representative characteristics of ISU required for wig applications. Although the properties of human hair differ slightly according to race and age, hair has diameters between 17 and 180 μm [53] and strengths in the 150–270 MPa range [47,48]. Human hair can be treated at fairly high temperatures (up to 200 °C) with applied external stress (human hand force), such as permanent waving, hair straightening, and curling. These properties are attributed to the unique structure of hair, which is composed of α-helix chains

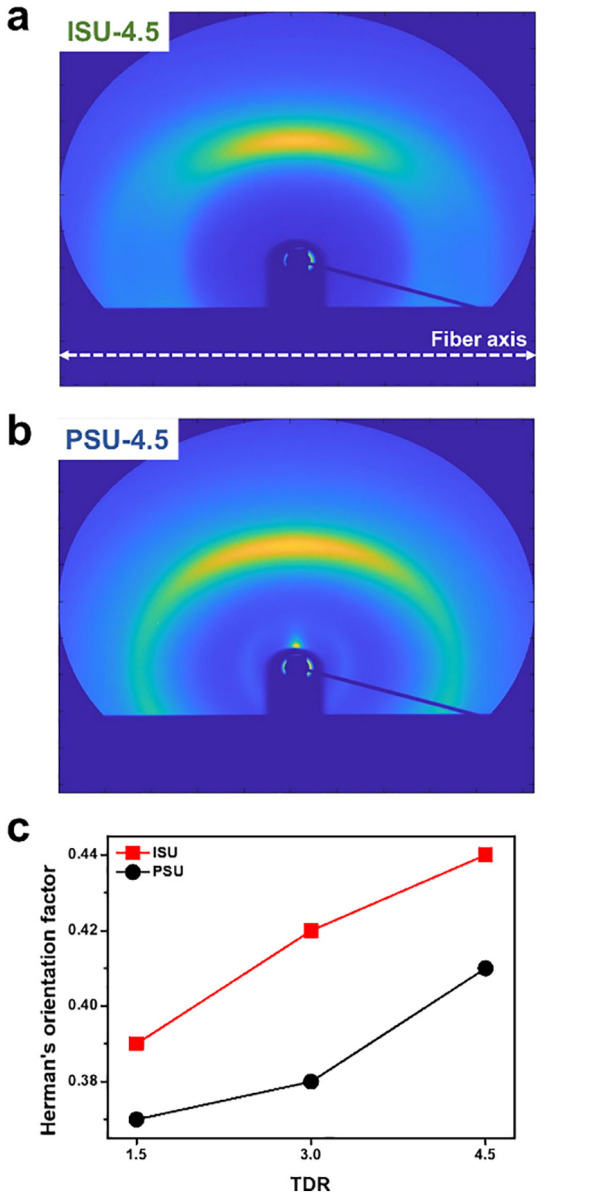

Fig. 5. 2D-WAXS images of (a) ISU-4.5 and (b) PSU-4.5. (c) Herman's orientation factors as functions of the total draw ratio.

(keratin) in crystalline microfibrils [52,64]. This structure prevents hair from thermally degrading at temperatures up to 250 °C. Artificial fibers used in wigs are fabricated mainly from PAN, PET, and PVC. These materials cannot withstand the high temperatures (>200 °C) required for hair treatment. Furthermore, studies regarding artificial fibers for wig applications, especially relevant to thermal analysis of the fibers, are very rare [35,36].

The thermally stable ISU-4.5 fibers are 40 μm in diameter and have a strength of 247 MPa (Fig. 2), which are well-matched to those of human hair. Hence, practical experiments were conducted using a hair iron to evaluate the potential of ISU-4.5 as a wig filament. Five bundles of 25-cm-long filaments were used in the hair iron experiments, with the fibers photographed and movies recorded. The temperature of the hair iron was set to 200 °C. Before any hair iron experiment, the bundles were stretched by hand to facilitate their use with the hair iron. Fig. 6a and Movie S4 show that ISU-4.5 does not break, even after being swept several times with hair iron. In contrast, PSU-4.5 broke as soon as it contacted the hair iron (Fig. 6b). The surfaces of the fibers were examined by SEM following hair iron experiments (Figs. 6d–g). ISU-4.5

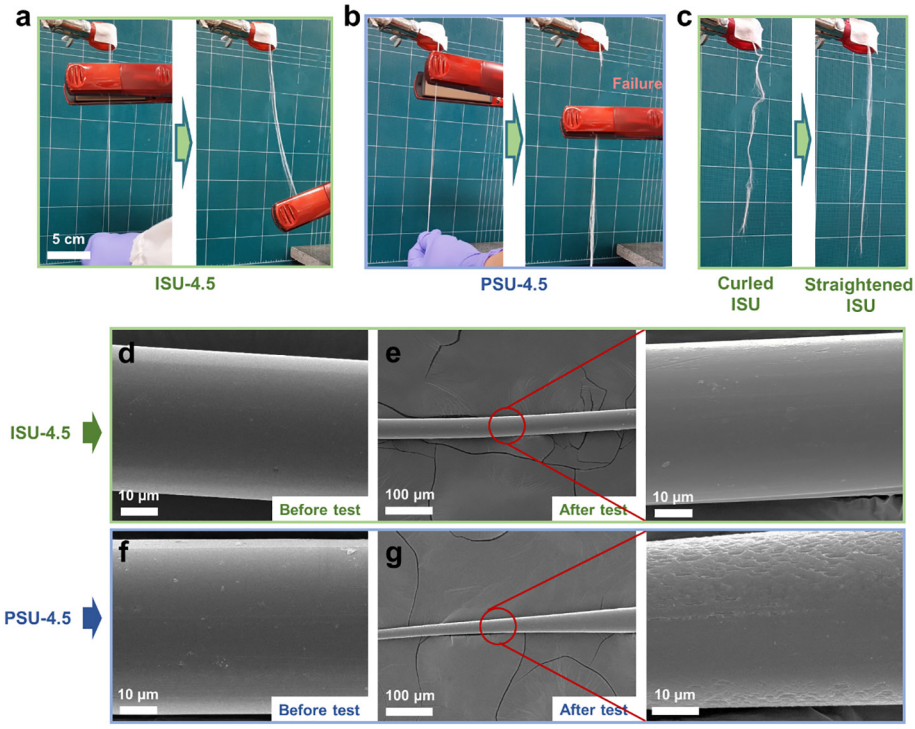

Fig. 6. Hair iron experiments using (a) ISU-4.5 and (b) PSU-4.5 (see Movie S4). (c) Straightening curled ISU-4.5 (see Movie S5). SEM images of (d, e) ISU-4.5 and (f, g) PSU-4.5 before and after the hair iron experiments.

showed smooth undamaged surfaces, similar to the original fibers; however, the SEM images of PSU-4.5 reveal necking in the area contacted by the hair iron. Moreover, it was confirmed that the surface was damaged, unlike that of the original PSU-4.5. As demonstrated in Fig. 6c and Movie S5, ISU-4.5 could be curled and then re-straightened after being swept with the hair iron.

To assess the abilities of these materials to be dyed, both ISU-4.5 and PSU-4.5 fibers were colored by brushing with black acrylic watercolor five times at 25 °C (Fig. 7a and Movie S6). Although acrylic watercolor is water-based, it is intrinsically resistant to water after drying. ISU-4.5 turned black after only a single brushing such that the original color of the fiber was not observed. However, PSU-4.5 still showed its original color even after five brushings. The fibers were then dried for 3 h under ambient conditions and washed in flowing water. While ISU-4.5 retained its blackness, without any color lost to the water, PSU-4.5 did not remain colored fully and showed its original white color in several places. The acrylic watercolor is more easily bound to ISU owing to the high number of oxygen atoms in its ISB units that can act as dyeing sites. Hence, the acrylic watercolor covered ISU-4.5 more homogeneously than PSU-4.5, as evidenced by the SEM images in Figs. 7b and c.

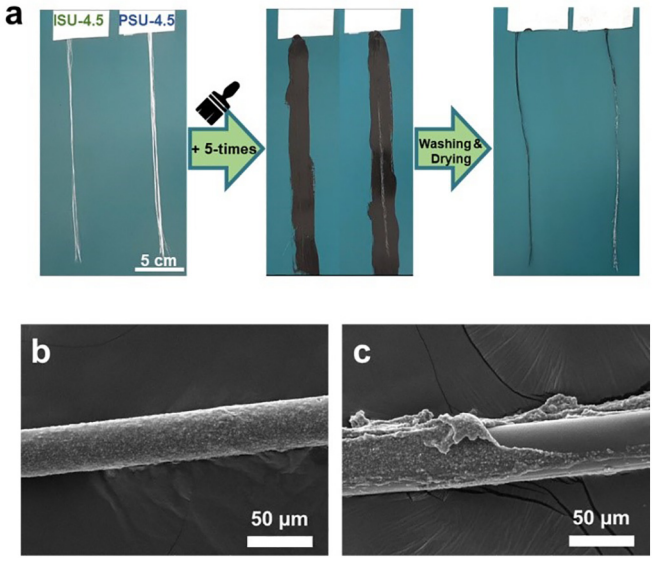

Fig. 7. (a) Coloring experiments using acrylic watercolor. SEM images of (b) ISU-4.5 and (c) PSU-4.5 after being colored (see Movie S6).

4. Conclusions

Bio-based fibers (ISUs) have been successfully fabricated using a dry-jet wet spinning process with ISB-based PAES as a partially biomass-derived amorphous SEP. The spinnability and physical properties of the ISUs were compared with those of petroleum derived BPA-based fibers (PSUs) using the same experimental conditions. The better tolerance of the ISB-PAES dope solution to water enables a compact fiber structure to form with remarkable orientational and mechanical properties compared to PSU. These properties are sufficient for the application of ISU to artificial hair. The high T_g enables ISU fibers to be curled and straightened using a hair iron without breakage. ISU was more uniformly colored with acrylic watercolor than PSU because of its partial hydrophilic and amorphous structure. Based on these properties, sustainable ISU is promising for use as a wig filament.

Supplementary data to this article can be found online at https://doi.org/10.1016/j.matdes.2020.109284.

Declaration of Competing Interest

The authors declare that they have no known competing financial interests or personal relationships that could have appeared to influence the work reported in this paper.

Acknowledgments

This work was supported by the Technology Innovation Program (10070150) funded by the Ministry of Trade, Industry & Energy (MI, Korea), and the Korea Research Institute of Chemical Technology (KRICT) core project (SS2042-10). We acknowledge the Pohang Accelerator Laboratory for X-ray diffractometry using synchrotron radiation (Beamline 3C). Special thanks to Jung-Eun Lee from UNIST, and Hyeonyeol Jeon, Jun Mo Koo, and Jonggeon Jegal from KRICT for their contribution to this study.

Data availability

The data that support the findings of this study are available from the corresponding author upon reasonable request.

References

[1] Editorial, The future of plastic, Nat. Commun. 9 (2018) 2157, https://doi.org/10.1038/s41467-018-04565-2.
[2] A. Scott, Tide will turn against single-use plastic, C&EN Glob. Enterp. 97 (2019) 36, https://doi.org/10.1021/cen-09702-cover5.
[3] C.E. Foulds, L.S. Treviño, B. York, C.L. Walker, Endocrine-disrupting chemicals and fatty liver disease, Nat. Rev. Endocrinol. 13 (2017) 445–457, https://doi.org/10.1038/nrendo.2017.42.
[4] X. Wu, S. Zheng, D.A. Bellido-Aguilar, V.V. Silberschmidt, Z. Chen, Transparent icephobic coatings using bio-based epoxy resin, Mater. Des. 140 (2018) 516–523, https://doi.org/10.1016/j.matdes.2017.12.017.
[5] S.H. Safe, Polychlorinated biphenyls (PCBs): environmental impact, biochemical and toxic responses, and implications for risk assessment, Crit. Rev. Toxicol. 24 (1994) 87–149, https://doi.org/10.3109/10408449409049308.
[6] J.C. Ramsey, M.E. Andersen, A physiologically based description of the inhalation pharmacokinetics of styrene in rats and humans, Toxicol. Appl. Pharmacol. 73 (1984) 159–175, https://doi.org/10.1016/0041-008X(84)90064-4.
[7] J.B. Zimmerman, P.T. Anastas, Toward substitution with no regrets, Science 347 (2015) 1198–1199, https://doi.org/10.1126/science.aaa0812.
[8] J.R. Rochester, Bisphenol A and human health: a review of the literature, Reprod. Toxicol. 42 (2013) 132–155, https://doi.org/10.1016/j.reprotox.2013.08.008.
[9] S. Lee, C. Kim, H. Shin, Y. Kho, K. Choi, Comparison of thyroid hormone disruption potentials by bisphenols A, S, F, and Z in embryo-larval zebrafish, Chemosphere 221 (2019) 115–123, https://doi.org/10.1016/j.chemosphere.2019.01.019.
[10] H.T.H. Nguyen, P. Qi, M. Rostagno, A. Feteha, S.A. Miller, The quest for high glass transition temperature bioplastics, J. Mater. Chem. A 6 (2018) 9298–9331, https://doi.org/10.1039/C8TA00377G.
[11] D.K. Schneiderman, M.A. Hillmyer, 50th anniversary perspective: there is a great future in sustainable polymers, Macromolecules 50 (2017) 3733–3749, https://doi.org/10.1021/acs.macromol.7b00293.
[12] S.-A. Park, Y. Eom, H. Jeon, J.M. Koo, E.S. Lee, J. Jegal, S.Y. Hwang, D.X. Oh, J. Park, Preparation of synergistically reinforced transparent bio-polycarbonate nanocomposites with highly dispersed cellulose nanocrystals, Green Chem. 21 (2019) 5212–5221, https://doi.org/10.1039/C9GC02253H.
[13] T. Kim, J.M. Koo, M.H. Ryu, H. Jeon, S.-M. Kim, S.-A. Park, D.X. Oh, J. Park, S.Y. Hwang, Sustainable terpolyester of high Tg based on bio heterocyclic monomer of dimethyl furan-2,5-dicarboxylate and isosorbide, Polymer 132 (2017) 122–132, https://doi.org/10.1016/j.polymer.2017.10.052.
[14] H.B. Abderrazak, A. Fildier, H.B. Romdhane, S. Chatti, H.R. Kricheldorf, Synthesis of new poly(ether ketone)s derived from biobased Diols, Macromol. Chem. Phys. 214 (2013) 1423–1433, https://doi.org/10.1002/macp.201300015.
[15] Y. Baimark, W. Rungseesantivanon, N. Prakymoramas, Improvement in melt flow property and flexibility of poly(l-lactide)-b-poly(ethylene glycol)-b-poly(l-lactide) by chain extension reaction for potential use as flexible bioplastics, Mater. Des. 154 (2018) 73–80, https://doi.org/10.1016/j.matdes.2018.05.028.
[16] T. Kim, H. Jeon, J. Jegal, J.H. Kim, H. Yang, J. Park, D.X. Oh, S.Y. Hwang, Trans crystallization behavior and strong reinforcement effect of cellulose nanocrystals on reinforced poly(butylene succinate) nanocomposites, RSC Adv. 8 (2018) 15389–15398, https://doi.org/10.1039/C8RA01868E.
[17] S.A. Park, H. Jeon, H. Kim, S.H. Shin, S. Choy, D.S. Hwang, J.M. Koo, J. Jegal, S.Y. Hwang, J. Park, D.X. Oh, Sustainable and recyclable super engineering thermoplastic from biorenewable monomer, Nat. Commun. 10 (2019) 2601, https://doi.org/10.1038/s41467-019-10582-6.
[18] S.A. Park, C. Im, D.X. Oh, S.Y. Hwang, J. Jegal, J.H. Kim, Y.W. Chang, H. Jeon, J. Park, Study on the synthetic characteristics of biomass-derived Isosorbide-based poly (arylene ether ketone)s for sustainable super engineering plastic, Molecules 24 (2019) 2492, https://doi.org/10.3390/molecules24132492.
[19] C. Dussenne, T. Delaunay, V. Wiatz, H. Wyart, I. Suisse, M. Sauthier, Synthesis of isosorbide: an overview of challenging reactions, Green Chem. 19 (2017) 5332–5344, https://doi.org/10.1039/C7GC01912B.
[20] Y. Zhu, M. Durand, V. Molinier, J.-M. Aubry, Isosorbide as a novel polar head derived from renewable resources. Application to the design of short-chain amphiphiles with hydrotropic properties, Green Chem. 10 (2008) 532–540 10.1039/B717203F.
[21] B.A. Howell, Y.G. Daniel, Isosorbide as a Platform for the Generation of New Biobased Organophosphorus Flame Retardants, Insi in Chem & Biochem. 1 (2020)https://irispublishers.com/icbc/fulltext/isosorbide-as-a-platform-for-the-generation-of-new-biobased-organophosphorus-flame-retardants.ID.000509.php.
[22] F. Aricò, Isosorbide as biobased platform chemical: recent advances, Curr. Opin. Green Sustain. Chem. 21 (2020) 82–88, https://doi.org/10.1016/j.cogsc.2020.02.002.
[23] Z. Saadatnia, S.G. Mosanenzadeh, E. Esmailzadeh, H.E. Naguib, A high performance Triboelectric Nanogenerator using porous polyimide aerogel film, Sci. Rep. 9 (2019) 1370, https://doi.org/10.1038/s41598-018-38121-1.
[24] X. Huang, Z. Zhang, X.-Y. Kong, Y. Sun, C. Zhu, P. Liu, J. Pang, L. Jiang, L. Wen, Engineered PES/SPES nanochannel membrane for salinity gradient power generation, Nano Energy 59 (2019) 354–362, https://doi.org/10.1016/j.nanoen.2019.02.056.
[25] X. Wang, M. Li, B.T. Golding, M. Sadeghi, Y. Cao, E.H. Yu, K. Scott, A polytetrafluoroethylene-quaternary 1,4-diazabicyclo-[2.2.2]-octane polysulfone composite membrane for alkaline anion exchange membrane fuel cells, Int. J. Hydrog Energy 36 (2011) 10022–10026, https://doi.org/10.1016/j.ijhydene.2011.05.054.
[26] BASF, Commercially available amorphous super engineering plastics: brochure from BASF, https://www.basf.com/global/documents/en/products-and-industries/car-interiorideal/2019/BASF_Ultrason_brochure.pdf 2019 (accessed 5 September 2020).
[27] Z. Zhang, X. Wang, G. Zu, K. Kanamori, K. Nakanishi, J. Shen, Resilient, fire-retardant and mechanically strong polyimide-polyvinylpolymethylsiloxane composite aerogel prepared via stepwise chemical liquid deposition, Mater. Des. 183 (2019) 108096, https://doi.org/10.1016/j.matdes.2019.108096.
[28] K. Stoeffler, S. Andjelic, N. Legros, J. Roberge, S.B. Schougaard, Polyphenylene sulfide (PPS) composites reinforced with recycled carbon fiber, Compos. Sci. Technol. 84 (2013) 65–71, https://doi.org/10.1016/j.compscitech.2013.05.005.
[29] S.-A. Park, Y. Eom, H. Jeon, J.M. Koo, T. Kim, J. Jeon, M.J. Park, S.Y. Hwang, B.-S. Kim, D.X. Oh, J. Park, Aramid nanofiber templated in situ SNAr polymerization for maximizing the performance of all-organic nanocomposites, ACS Macro Lett. 9 (2020) 558–564, https://doi.org/10.1021/acsmacrolett.0c00156.
[30] M.A. Hickner, H. Ghassemi, Y.S. Kim, B.R. Einsla, J.E. McGrath, Alternative polymer Systems for Proton Exchange Membranes (PEMs), Chem. Rev. 104 (2004) 4587–4612, https://doi.org/10.1021/cr020711a.
[31] J. Lee, J. Park, J. Oh, S. Lee, S.Y. Kim, M. Seo, Nanoporous poly(ether sulfone) from polylactide-b-poly(ether sulfone)-b-polylactide precursor, Polymer 180 (2019) 121704, https://doi.org/10.1016/j.polymer.2019.121704.
[32] J.-E. Lee, Y.E. Kim, G.-H. Lee, M.J. Kim, Y. Eom, H.G. Chae, The effect of cellulose nanocrystals (CNCs) on the microstructure of amorphous polyetherimide (PEI)-based nanocomposite fibers and its correlation with the mechanical properties, Compos. Sci. Technol. 200 (2020) 108452, https://doi.org/10.1016/j.compscitech.2020.108452.
[33] T.V. Sreekumar, T. Liu, B.G. Min, H. Guo, S. Kumar, R.H. Hauge, R.E. Smalley, Polyacrylonitrile single-walled carbon nanotube composite fibers, Adv. Mater. 16 (2004) 58–61, https://doi.org/10.1002/adma.200305456.
[34] Y. Liu, H.C. Kim, Y.S. Chung, Basic study on the two-tone color dyeing of PET and PVC wig fibers by carrier dyeing method, Fiber. Polym. 8 (2007) 363–371, https://doi.org/10.1007/BF02875824.
[35] L. Yang, J. Guo, S. Zhang, Y. Gong, Preparation and characterization of novel super-artificial hair fiber based on biomass materials, Int. J. Biol. Macromol. 99 (2017) 166–172, https://doi.org/10.1016/j.ijbiomac.2017.02.077.
[36] Y.W. Park, I.J. Song, H.C. Kim, Characterization of PET/PP blend fiber and it's application to wig, Fiber. Polym. 15 (2014) 1078–1083, https://doi.org/10.1007/s12221-014-1078-y.
[37] M. Joshi, Nanotechnology in Textiles: Advances and Developments in Polymer Nanocomposites, CRC Press, 2020 Chapter 5.5.
[38] B. Elvers, F. Ullmann, Ullmann's Polymers and Plastics: Products and Processes, Wiley-VCH Verlag GmbH & Company KGaA, 2020 1523–1524.
[39] I.S. Kim, H.M. Cho, J. Koh, J.P. Kim, Low-temperature carrier dyeing of poly(vinyl chloride) fibers with disperse dyes, J. Appl. Polym. Sci. 90 (2003) 3896–3904, https://doi.org/10.1002/app.13180.
[40] A.E.A. Elabid, J. Zhang, J. Shi, Y. Guo, K. Ding, J. Zhang, Improving the low temperature dyeability of polyethylene terephthalate fabric with dispersive dyes by atmospheric pressure plasma discharge, Appl. Surf. Sci. 375 (2016) 26–34, https://doi.org/10.1016/j.apsusc.2015.12.015.
[41] X. Li, Y. Yang, H. Zhang, Z. Quan, X. Qin, F. Li, R. Wang, J. Yu, Modified polyacrylonitrile nanofibers for improved dyeability using anionic dyes, Appl. Nanosci. 10 (2020) 2025–2035, https://doi.org/10.1007/s13204-020-01380-4.
[42] A.S. Abdel-Naby, S.N. Al-Harthi, Dyeability and mechanical properties of acrylonitrile-diallylamine salts copolymers, Am. J. Appl. Sci. 10 (2013) 525, https://doi.org/10.3844/ajassp.2013.525.535.
[43] Y.-Z. Wang, S.-P. Du, X.-Y. Shen, L.-W. Zhu, Z.-P. Gong, Acid-dye-dyeable polyacrylonitrile/ poly(N,N-dilkylaminoethylacrylate) acrylic blend fiber, J. Appl. Polym. Sci. 106 (2007) 84–88, https://doi.org/10.1002/app.26498.
[44] M.M. Hirschler, Hydrogen chloride evolution from the heating of poly(vinyl chloride) compounds, Fire. Mater. 29 (2005) 367–382, https://doi.org/10.1002/fam.893.
[45] Z. Hajalifard, F. Rashidi, R. Badrnezhad, Hydrogen Cyanide Formation in PAN Carbon Fiber Furnaces, The 8th International Chemical Engineering Congress & Exhibition (IChEC2014), http://www.sid.ir/FileServer/SE/219e201408762 2014.
[46] M. Zimmerley, C.-Y. Lin, D. Oertel, J. Marsh, J. Ward, E. Potma, Quantitative detection of chemical compounds in human hair with coherent anti-stokes Raman scattering microscopy, J. Biomed. Opt. 14 (2009), 044019, https://doi.org/10.1117/1.3184444.
[47] Y. Yu, W. Yang, B. Wang, M.A. Meyers, Structure and mechanical behavior of human hair, Mater. Sci. Eng. C 73 (2017) 152–163, https://doi.org/10.1016/j.msec.2016.12.008.

[48] L.J. Wolfram, Human hair: A unique physicochemical composite, J. Am. Acad. Dermatol. 2003 (48) (2003) S106–S114, https://doi.org/10.1067/mjd.2003.276.
[49] J.C. Lim, Y.W. Park, H.C. Kim, Study on manufacturing PCT/PPS flame retardant Fiber by sheath/core conjugate spinning, Fiber. Polym. 21 (2020) 498–504, https://doi.org/10.1007/s12221-020-9082-x.
[50] B.A. Newcomb, H.G. Chae, L. Thomson, J. Luo, J.-B. Baek, S. Kumar, Reinforcement efficiency of carbon nanotubes and their effect on crystal-crystal slip in poly(ether ketone)/carbon nanotube composite fibers, Compos. Sci. Technol. 147 (2017) 116–125, https://doi.org/10.1016/j.compscitech.2017.05.011.
[51] R. Jain, Y.H. Choi, Y. Liu, M.L. Minus, H.G. Chae, S. Kumar, J.-B. Baek, Processing, structure and properties of poly(ether ketone) grafted few wall carbon nanotube composite fibers, Polymer. 51 (2010) 3940–3947, https://doi.org/10.1016/j.polymer.2010.06.034.
[52] C. Kunchi, K.C. Venkateshan, N.D. Reddy, R.B. Adusumalli, Correlation between mechanical and thermal properties of human hair, Int. J. Trichol. 10 (2018) 204–210, https://doi.org/10.4103/ijt.ijt_24_18.
[53] B. Ley, Diameter of a Human Hair, The Physics Factbook https://hypertextbook.com/facts/1999/BrianLey.shtml 1991 (accessed 5 September 2020).
[54] J. Kaur, K. Millington, S. Smith, Producing high-quality precursor polymer and fibers to achieve theoretical strength in carbon fibers: a review, J. Appl. Polym. Sci. 133 (2016)https://doi.org/10.1002/app.43963.
[55] J.H. Yoon, S.-M. Kim, Y. Eom, J.M. Koo, H.-W. Cho, T.J. Lee, K.G. Lee, H.J. Park, Y.K. Kim, H.-J. Yoo, S.Y. Hwang, J. Park, B.G. Choi, Extremely fast self-healable bio-based supramolecular polymer for wearable real-time sweat-monitoring sensor, ACS Appl. Mater. Interfaces 11 (2019) 46165–46175, https://doi.org/10.1021/acsami.9b16829.
[56] D.W. Van Krevelen, K. Te Nijenhuis, Chapter 7 - cohesive properties and solubility, in: D.W. Van Krevelen, K. Te Nijenhuis (Eds.), Properties of Polymers (Fourth Edition), Amsterdam, Elsevier 2009, pp. 189–227.
[57] H. Kim, T. Kim, S. Choi, H. Jeon, D.X. Oh, J. Park, Y. Eom, S.Y. Hwang, J.M. Koo, Remarkable elasticity and enzymatic degradation of bio-based poly(butylene adipate-co-furanoate): replacing terephthalate, Green Chem. (2020)https://doi.org/10.1039/D0GC01688H.
[58] W.J. Yoon, S.Y. Hwang, J.M. Koo, Y.J. Lee, S.U. Lee, S.S. Im, Synthesis and characteristics of a biobased high-Tg Terpolyester of Isosorbide, ethylene glycol, and 1,4-cyclohexane dimethanol: effect of ethylene glycol as a chain linker on polymerization, Macromolecules 46 (2013) 7219–7231, https://doi.org/10.1021/ma4015092.
[59] J.P. Knudsen, The influence of coagulation variables on the structure and physical properties of an acrylic fiber, Text. Res. J. 33 (1963) 13–20, https://doi.org/10.1177/004051756303300103.
[60] S.H. Bahrami, P. Bajaj, K. Sen, Effect of coagulation conditions on properties of poly (acrylonitrile–carboxylic acid) fibers, J. Appl. Polym. Sci. 89 (2003) 1825–1837, https://doi.org/10.1002/app.12275.
[61] H.-S. Yang, Y.-M. Kim, H. Choi, J. Jang, J.H. Youk, B.-S. Lee, W.-R. Yu, Electrochemical wet-spinning process for fabricating strong PAN fibers via an in situ induced plasticizing effect, Polymer 202 (2020) 122641, https://doi.org/10.1016/j.polymer.2020.122641.
[62] L. Sun-Nye, A study of characteristics of Wft used in wig manufacturing, Text. Coloration Finish. 24 (2012) 204–213, https://doi.org/10.5764/TCF.2012.24.3.204.
[63] S.-A. Park, J. Choi, S. Ju, J. Jegal, K.M. Lee, S.Y. Hwang, D.X. Oh, J. Park, Copolycarbonates of bio-based rigid isosorbide and flexible 1,4-cyclohexanedimethanol: merits over bisphenol-a based polycarbonates, Polymer 116 (2017) 153–159, https://doi.org/10.1016/j.polymer.2017.03.077.
[64] V. Monteiro, F. Ria, A.P. Maciel, E. Longo, Thermal analysis of caucasian human hair, J. Therm. Anal. Calorim. 79 (2005) 289–293, https://doi.org/10.1007/s10973-005-0051-9.